

Enhancement of U4/U6 Small Nuclear Ribonucleoprotein Particle Association in Cajal Bodies Predicted by Mathematical Modeling

Mirko Klingauf,* David Staněk,[†] and Karla M. Neugebauer

Max Planck Institute of Molecular Cell Biology and Genetics, 01307 Dresden, Germany

Submitted June 9, 2006; Revised July 26, 2006; Accepted September 8, 2006
Monitoring Editor: A. Gregory Matera

Spliceosomal small nuclear ribonucleoprotein particles (snRNPs) undergo specific assembly steps in Cajal bodies (CBs), nonmembrane-bound compartments within cell nuclei. An example is the U4/U6 di-snRNP, assembled from U4 and U6 monomers. These snRNPs can also assemble in the nucleoplasm when cells lack CBs. Here, we address the hypothesis that snRNP concentration in CBs facilitates assembly, by comparing the predicted rates of U4 and U6 snRNP association in nuclei with and without CBs. This was accomplished by a random walk-and-capture simulation applied to a three-dimensional model of the HeLa cell nucleus, derived from measurements of living cells. Results of the simulations indicated that snRNP capture is optimal when nuclei contain three to four CBs. Interestingly, this is the observed number of CBs in most cells. Microinjection experiments showed that U4 snRNA targeting to CBs was U6 snRNP independent and that snRNA concentration in CBs is ~20-fold higher than in nucleoplasm. Finally, combination of the simulation with calculated association rates predicted that the presence of CBs enhances U4 and U6 snRNP association by up to 11-fold, largely owing to this concentration difference. This provides a chemical foundation for the proposal that these and other cellular compartments promote molecular interactions, by increasing the local concentration of individual components.

INTRODUCTION

Cajal bodies (CBs) are evolutionarily conserved, nonmembrane-bound compartments, in which components of the pre-mRNA splicing, histone mRNA 3' end formation, and pre-rRNA processing machineries are concentrated (Gall, 2000; Matera and Shpargel, 2006; Stanek and Neugebauer, 2006). Most somatic cells contain two to four CBs, 0.5–1.0 μm in diameter, which are most prominently marked by the CB-specific protein coilin. Recent studies have shown that CB components reside for relatively short times in CBs, suggesting that molecular events occur in CBs in the context of a dynamic exchange of factors with the surrounding nucleoplasm (Handwerger *et al.*, 2003; Dundr *et al.*, 2004). In addition, CBs themselves are highly dynamic, in that they move, split, and fuse during the lifetime of the cell (Andrade *et al.*, 1993; Boudonck *et al.*, 1999; Platani *et al.*, 2000); moreover, their structure is dependent on active transcription and metabolic activity, suggesting that a constant supply of substrates is required to maintain CB integrity (Carmo-Fonseca *et al.*, 1992; Boudonck *et al.*, 1998; Shpargel and Matera, 2005; Lemm *et al.*, 2006). Although it is formally possible that the occurrence of CBs in nuclei is an indirect outcome of physiological state, speculation has focused in recent years on the

possibility that concentration of components facilitates key steps in gene expression. However, the chemical underpinnings of the latter hypothesis have not been addressed thus far.

Studies on the biogenesis of spliceosomal small nuclear ribonucleoprotein particles (snRNPs), which are essential factors in pre-mRNA splicing, have revealed that numerous steps occur in the CB. Each snRNP consists of a small U-rich RNA complexed with a number of specific snRNP proteins. During snRNP assembly, each of the five spliceosomal snRNAs—U1, U2, U4, U5, and U6—receives a stable heptameric ring of small proteins, named Sm proteins for all snRNAs except for U6 that receives a ring of related Lsm proteins (Matera and Shpargel, 2006; Stanek and Neugebauer, 2006). These “core” snRNPs subsequently assemble with multiple snRNP-specific proteins in the nucleus, and the snRNPs further mature by additional assembly steps. For example, the U4 and U6 snRNPs associate and, through base pairing between the U4 and U6 snRNAs, form the U4/U6 di-snRNP. Subsequently, the di-snRNP associates with the U5 snRNP through protein–protein interactions, to form the U4/U6·U5 tri-snRNP. Recent observations show that U4/U6 snRNP assembly, as well as U4/U6·U5 tri-snRNP formation occur in the CB (Stanek *et al.*, 2003; Schaffert *et al.*, 2004; Stanek and Neugebauer, 2004). Similarly, the U2 snRNP seems to undergo specific assembly steps in the CB (Nesic *et al.*, 2004). In addition, snRNA targeting to the CB is required for nucleotide modifications, which are guided by the small Cajal body-specific RNAs (Darzacq *et al.*, 2002; Kiss *et al.*, 2002; Jady *et al.*, 2003). The independent targeting to CBs of the many distinct components involved suggests that CBs coordinate multiple steps in the snRNP biogenesis pathway (Matera and Shpargel, 2006; Stanek and Neugebauer, 2006).

This article was published online ahead of print in *MBC in Press* (<http://www.molbiolcell.org/cgi/doi/10.1091/mbc.E06-06-0513>) on September 20, 2006.

Present addresses: *Institute of Biochemistry, ETH-Zurich, 8093 Zurich, Switzerland; [†]Department of Cellular Biology and Pathology, First Medical Faculty of Charles University in Prague, 128 00 Prague, Czech Republic.

Address correspondence to: Karla M. Neugebauer (neugebau@mpi-cbg.de).

Progress on identifying the molecular functions that occur in CBs provides an entry point for considering how CBs might promote key events in gene expression. In the present study, we consider the assembly of the U4/U6 snRNP, which occurs preferentially in CBs. However, in cells depleted of the protein coilin, snRNPs are dispersed, and elevated nucleoplasmic levels of U4/U6 snRNP assembly are detected (Stanek and Neugebauer, 2004). This raises the possibility that U4/U6 snRNPs can assemble in the nucleoplasm but that they may do so with greater efficiency in CBs, if present. Therefore, we have applied mathematical modeling to predict answers to the following questions: Do U4 and U6 snRNPs associate more efficiently if they first concentrate in CBs? Or, alternatively, is U4-U6 snRNP association by random walk throughout the nucleoplasm sufficiently rapid that concentration of snRNPs in CBs provides no advantage for snRNP assembly? We assume that the snRNPs move by diffusion within the nucleus, because the majority of previous studies have pointed to a lack of metabolic energy for intranuclear movements of proteins and RNAs (Misteli *et al.*, 1997; Kues *et al.*, 2001; Calapez *et al.*, 2002; Dundr *et al.*, 2004; Shav-Tal *et al.*, 2004; Politz *et al.*, 2006). To accomplish our aim, we determined the concentration difference for snRNAs in the CB versus nucleoplasm and derived a three-dimensional model of the living HeLa cell nucleus. We find that, given random walk kinetics through the entire volume of the HeLa cell nucleus, the concentration difference drives up to 11-fold enhanced rates of snRNP assembly in nuclei containing CBs.

MATERIALS AND METHODS

Antibodies and Plasmids

Monoclonal antibody (mAb) 5P10 (Almeida *et al.*, 1998) specific for human coilin was a gift of Maria Carmo-Fonseca (Institute of Molecular Medicine, Faculty of Medicine, University of Lisbon, Lisbon, Portugal). mAb 17C12 specific for fibrillarin was from Eng Tan (W.M. Keck Autoimmune Disease Center, Department of Molecular and Experimental Medicine, The Scripps Research Institute, La Jolla, CA). Secondary anti-mouse and anti-rabbit antibodies conjugated to Cy5 were obtained commercially (Jackson ImmunoResearch Laboratories, West Grove, PA). The squamous cell carcinoma antigen recognized by T cells 3-enhanced green fluorescent protein (SART3-EGFP-C3) expression vector was described previously (Stanek *et al.*, 2003).

In Vitro Transcription and Labeling of RNA

A wild-type human U4 snRNA clone (U4C) (Wersig and Bindereif, 1990) was used as a template for polymerase chain reaction (PCR) and in vitro transcription with the following primers (italics show T7 promoter): 5'-TAATACGACTACTATAGGG/AGCTTTGGCCAGTGGCAGTAT-3' (T7-U4wt 5), 5'-CAGTCTCCGTAGAGACTGTCA-3' (U4wt-3'), 5'-TAATACGACTACTATAGGG/TATCGTAGCCAATGAGGTTAATCCGAGGCGCGGATTAT-3' (T7-U4Δ1-18/56-63-5'), and 5'-CAGTCTCCGTAGAGACTGTGGCCGCCGCCCAATGCCGAC-3' (U4sub5m-3').

All RNA transcripts were obtained using a T7 driven in vitro transcription kit (MEGAscript; Ambion, Austin, TX) and labeled with Alexa 488 rUTPs (Invitrogen, Carlsbad, CA). Their ends contained a GG from the T7 promoter, so that all snRNA transcripts could be capped additionally with m⁷G(5')ppp(5')G (Ambion). One transcription reaction of 10 μl contained 1 mM ATP, 1 mM CTP, 0.45 mM rGTP, 1.8 mM m⁷G(5')ppp(5')G cap analog, 0.8 mM UTP, 0.2 mM Alexa 488-labeled UTP, 100–200 ng of U4C template, and 1 μl MEGAscript enzyme mix in 1X transcription buffer provided by the manufacturer. After 3- to 4-h incubation in a 37°C waterbath, 1 μl of RNase-free DNase was added, mixed, and incubated for 30 min under the same conditions. Subsequently, the RNA was purified using the MEGAclear RNA purification kit (Ambion). The purified RNA was precipitated with ethanol, dried, and resuspended in 12 μl of microinjection buffer (10 mM Tris, pH 7.4, and 70 mM KCl). The integrity of the in vitro-transcribed RNA was confirmed by electrophoresis. RNA concentrations were measured using an Ultraspec 3100 proUV/Vis (Biochrome, Cambridge, United Kingdom). Concentrations of RNAs for injection were adjusted to 200 ng/μl.

Microinjection

HeLa cells were microinjected on a Zeiss Axiovert 200 M microscope with a 40× long-distance objective. Injection was carried out using an Eppendorf

MicroJet ($P_{\text{inject}} = 150$ hPa; $P_{\text{capillary}} = 50$ hPa) equipped with sterile Femtotips II (Eppendorf, Hamburg, Germany) and a micromanipulator (Leica, Wetzlar, Germany). The needle was manually moved, and cell contact lasted for ~0.5 s. After microinjection, cells were incubated at 37°C for 30–90 min to recover and then fixed.

Immunostaining

For immunostaining, cells were washed three times with 10 mM MgCl₂ and phosphate-buffered saline (MgPBS) after each fixation step. Cells were fixed in 4% paraformaldehyde (PFA) [4% PFA, 0.1 M piperazine-*N,N'*-bis(2-ethanesulfonic acid), pH 6.9, 2 mM MgCl₂, 1.25 mM EGTA, and distilled H₂O] for 10 min at room temperature (RT). Permeabilization was carried out for 10 min with 0.2% Triton X-100 in MgPBS. The blocking step was conducted by incubating in 5% normal goat serum (Sigma-Aldrich, St. Louis, MO) in MgPBS. Immunostaining of Cajal bodies was performed, using coilin-specific mAb 5P10 diluted 1:1000 and 17C12 diluted 1:10 in 3% BSA for 1 h at RT, followed by Cy5-anti-mouse secondary antibodies. Coverslips were mounted in 95% glycerol with 4,6-diamidino-2-phenylindole and 1,4-diazabicyclo[2.2.2]octane (Invitrogen).

Microscopy of Fixed Samples and Image Analysis

Images of fixed and immunostained cells were collected using the DeltaVision microscope system (Applied Precision, Seattle, WA) coupled with an Olympus IX70 microscope. Stacks of 25 sections in the z-direction with 200-nm z-steps were taken from each cell by using a 100×/1.4 numerical aperture (NA) PlanApo oil immersion objective. Collected data were then subjected to deconvolution using softWoRx (Applied Precision) software. To determine the enrichment of the different snRNAs in CBs compared with the nucleoplasm, the section with the highest intensity for each CB, assuming that this is the middle plane, was analyzed. The intensities of the CBs, nucleoplasm, and background were measured. The data were first analyzed by calculating the average intensity per pixel of the region of interest (ROI). Next, the values were normalized according to the following equation:

$$\text{Ratio} = \frac{I_{\text{MeanROI}} - I_{\text{MeanBG}}}{I_{\text{MeanNP}} - I_{\text{MeanBG}}}$$

where I_{MeanROI} is the mean intensity, I_{MeanBG} is the average intensity outside of the cell, and I_{MeanNP} is the average intensity in the nucleoplasm of the same cell.

To measure the intensity of the total fluorescence injected into the whole cell, all 25 sections of the deconvolved image were projected into one plane. Measuring an ROI containing the whole cell including the cytoplasm yielded the integrated intensity of the ROI (I_{ROI}). To correct for the background signal, another region outside the cell was measured that gave the integrated intensity of a background ROI (I_{BG}). Finally, the injected integrated intensity of a cell (I_{Cell}) could be calculated by

$$\sum I_{\text{Cell}} = \sum I_{\text{ROI}} - \frac{A_{\text{ROI}}}{A_{\text{BG}}} \sum I_{\text{BG}}$$

where A_{ROI} and A_{BG} are the corresponding areas.

Live Cell Imaging and Data Analysis

For transfection, HeLa cells were grown on glass-bottomed microwell dishes (MatTek, Ashland, MA) for 24–48 h, until the cell density reached 50–70%. FuGene 6 (Roche Diagnostics, Mannheim, Germany) was used for transfection of cells with 1 μg of SART3-EGFP plasmid DNA and analyzed 16–24 h posttransfection. Live cells were imaged at 37°C by using a Bachhoffer chamber (Carl Zeiss, Jena, Germany) placed on a Saur heated frame (Helmut Saur, Reutlingen, Germany). Images were acquired on a LSM 510 (Carl Zeiss) with a C-Apochromat 63×/1.2NA water immersion objective. Green fluorescent protein (GFP) fluorescence was detected using a 488-nm excitation line of an Argon laser (30-mW nominal output) and a long pass 505 filter. Approximately 100 sections in the z-direction (distance between two stacks, 100 nm) were taken of each cell, and three-dimensional images of 25 cells were analyzed. Images were processed and analyzed with MetaView software (Carl Zeiss) by using the 3D distance tool to measure the semiaxes of the nucleus and the corresponding nucleoli. Briefly, the longest axis of each nucleus was measured, followed by the longest axis perpendicular to the first. Finally, the longest perpendicular distance in z direction was measured. The same was done for nucleoli. From these parameters, the average axis lengths were calculated. For nucleoli, the axes were used to calculate individual volumes that were summed for every cell (total nucleolar volume) and averaged over all cells. For the model, the axes ratio of the nucleus (388:276:100 = 10.1 μm:6.1 μm:2.6 μm) was applied to the volume of the nucleoli, to prevent distortion. Finally, the axes were recalculated (using the ratio of the nuclear and nucleolar volumes), and a single nucleolus representing the total volume of all the nucleoli was placed in the middle of the simulated nucleus.

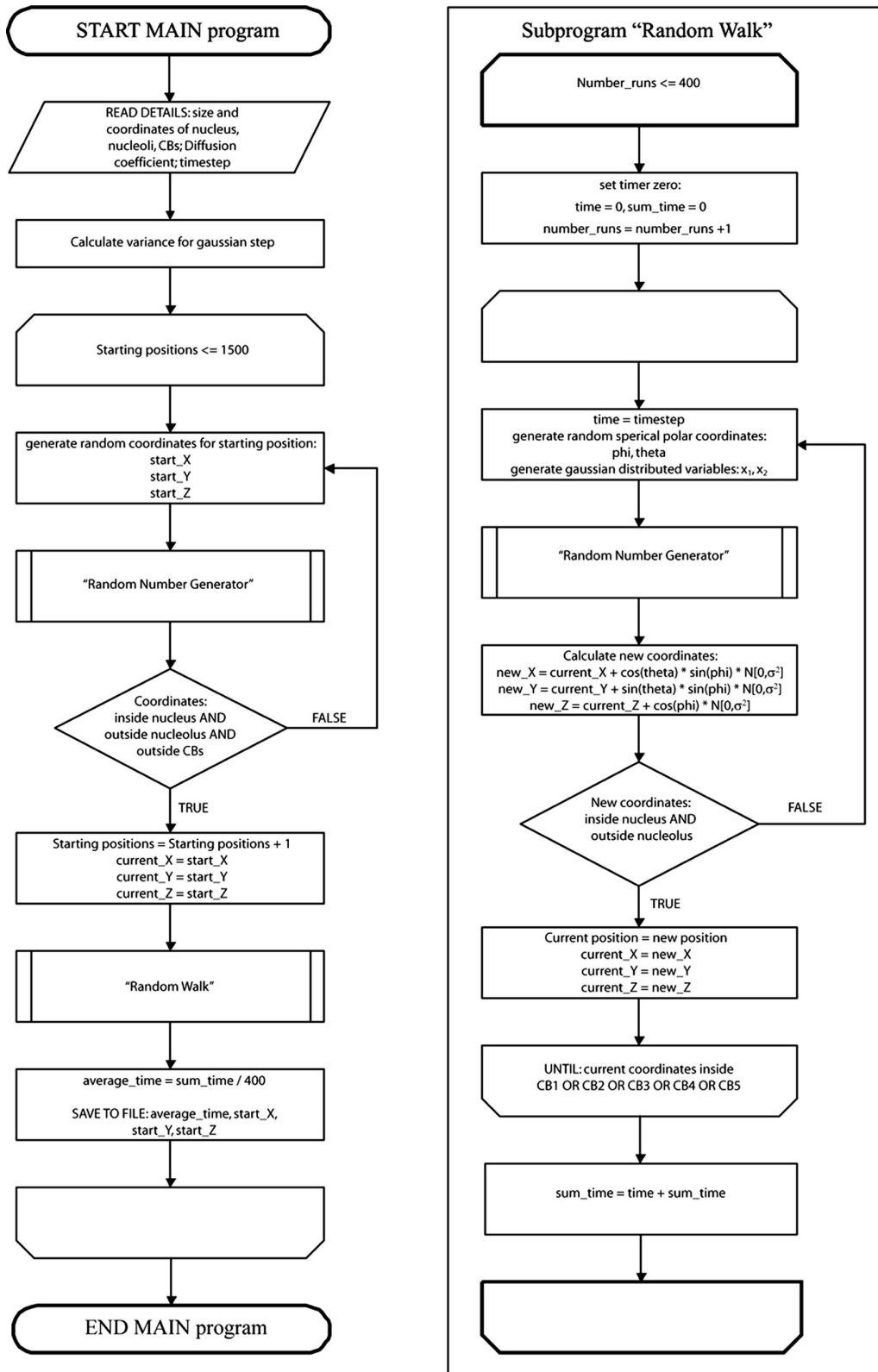


Figure 1. Flow chart of simulation in a nucleus with up to five CBs. Chart is showing the main program on the left and the subprogram Random Walk on the right side.

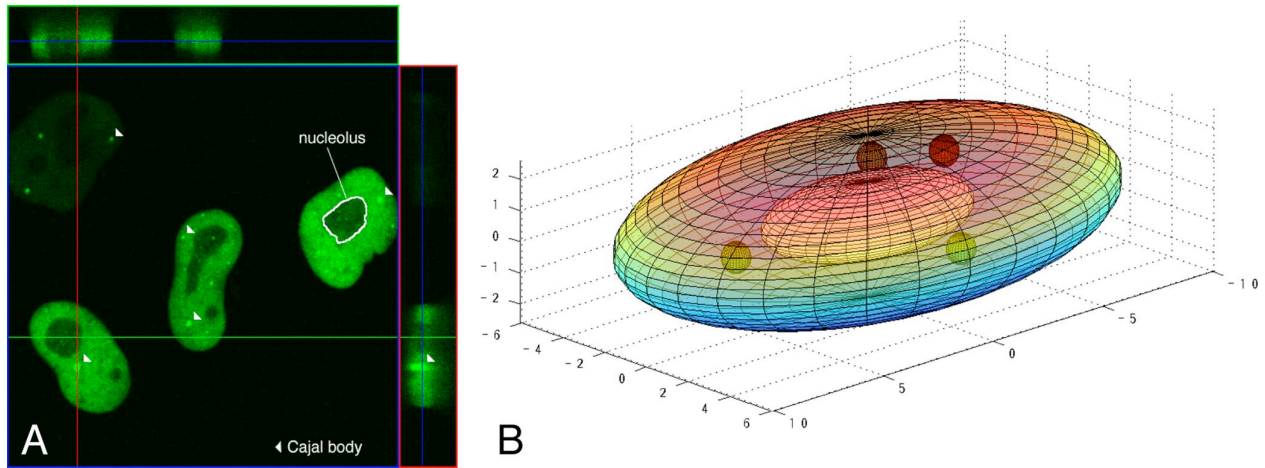


Figure 2. Three-dimensional modeling of an average, living HeLa cell nucleus. (A) HeLa cells were transfected with SART3-GFP. Twenty-four hours posttransfection, live cells were imaged using a Zeiss LSM 510 microscope. Approximately 100 sections in the z-direction were taken. An image created by MetaView software (Carl Zeiss) shows sections of a cell in the xz plane (top green box), yz plane (right red box) and xy plane (big blue box). The distance tool was used in this environment to determine the dimensions of HeLa cell nuclei. SART3-GFP is almost entirely found in the nucleoplasm, concentrated in CBs (arrowheads), and excluded from nucleoli. The display window shows an area of $73 \times 73 \mu\text{m}$ and includes cells expressing different levels of SART3-GFP. (B) Three-dimensional projection of the average HeLa cell nucleus including one nucleolus and CBs. Axis scale in micrometers.

Simulation of snRNP Association in the Nucleus by Using a Random Walk

The random walk method (Berg, 1993) in three dimensions ($m = 3$) starts always at a random position within the cell nucleus but outside CBs and the nucleolus. The particles undergo a three-dimensional random walk by changing their position at each positive integer n according to the following equation:

$$x^{n+1} = x^n + N^n(\mu, 2mD\delta t)$$

where $N^n(\mu, 2mD\delta t)$ is a vector of independent, identically distributed Gaussian random numbers with each element having a mean of $\mu = 0$ and the variance $2mD\delta t$. D is the molecular diffusion constant ($D = 1 \mu\text{m}^2/\text{s}$; $0.5 \mu\text{m}^2/\text{s}$; $0.2 \mu\text{m}^2/\text{s}$), and δt is the simulation time step ($\delta t = 10^{-3}$ s). As boundary condition, the nuclear membrane and nucleolus were treated as reflective barriers. Simulation was stopped when the particle was absorbed by a CB. Four hundred runs of one random starting position were averaged to yield a representative mean first passage time for the particular position. This was done for 1500 random starting positions within the nucleus, and all values were averaged to yield the mean first passage time for our particular geometrical model of a cell nucleus. A flow chart of the simulation is diagrammed in Figure 1.

Estimation of Association Rates

Suppose particle A has a radius of R_A , target particle B has a radius of R_B , adsorption takes place whenever they touch, and they can diffuse freely having a diffusion coefficient of D_A and D_B , respectively. Then, the collision rate is calculated by

$$k_D = 4\pi(D_A + D_B)(R_A + R_B)$$

which is called Smoluchowski result. To convert this value to a more commonly used unit ($\text{M}^{-1} \text{s}^{-1}$) it is multiplied with $1000 \times N_A$ (Avogadro's constant) (Howard, 2001). The use of $R_A = R_B = 3.5$ nm as radius for snRNPs (Stark *et al.*, 2001) and a diffusion coefficient of $D_A = D_B = 0.5 \mu\text{m}^2/\text{s}$ yields the diffusion-limited association rate of $k_D = 5.3 \times 10^7 \text{M}^{-1} \text{s}^{-1}$. This would be the association rate if every hit were productive.

Proteins in solution show a different behavior. First, only small "patches" on the protein surface are active and lead, in proper orientation, to a successful interaction. Second, it has been shown by Brownian dynamics simulation that multiple collisions between the same molecules can occur, which facilitates the exploration of a substantial fraction of protein surfaces, enhancing the possibility of a correct orientation (Northrup and Erickson, 1992).

To account for these two factors, the molecules were treated as spheres and a so-called patch factor (f_{patch}) given by

$$f_{\text{patch}} = \frac{\delta_A \delta_B (\delta_A + \delta_B)}{8}$$

was applied where "reactive" patches are spanned by the polar angles (θ , δ_A) and (θ , δ_B) on the sphere's surface (Berg, 1985; Zhou, 1993; Vijayakumar *et al.*, 1998). For $\delta_A = \delta_B = 3^\circ$, the association rate is lowered roughly by the same magnitude shown for proteins in solution with high ionic strength (Schreiber and Fersht, 1996).

$$k_{\text{patch}} = f_{\text{patch}} \cdot k_D$$

To apply these equations to our model, the approximate number of unbound U6 snRNPs in the nucleus ($1/3$ of 4×10^5 ; Yu *et al.*, 1999) and the accessible volume of our model HeLa cell nucleus ($\approx 620 \mu\text{m}^3$) were used to calculate the target concentration in nucleoplasm (4×10^{-7} M). Multiplying this value with k_{patch} yielded the association rates in the nucleoplasm (k_{NP}) and within CBs (k_{CB}). The calculated values are shown in Table 2. Finally, the calculated association rates can be combined with the simulation results and directly compared with the association occurring in nuclei without CB.

RESULTS

To apply mathematical modeling to the problem of U4 and U6 snRNA association in the HeLa cell nucleus, we set out to determine how a single U4 snRNA might encounter U6 snRNAs as it diffuses within the nucleus. We chose this strategy, because the number of U4 mono-snRNPs is too low to be estimated, whereas U6 snRNPs are relatively abundant and the number can be calculated (see below). First, the volume of the nucleus available for snRNA exploration had to be determined. It was important to perform this analysis on living cells because fixation can cause shrinkage or distortion of cellular structures. Therefore, HeLa cells were transfected with GFP-tagged SART3 (Figure 2A), which is distributed throughout the nucleoplasm and concentrated in CBs but excluded from nucleoli (Stanek *et al.*, 2003). Because SART3 is a component of the U6 snRNP as well as the U4/U6 di-snRNP (Bell *et al.*, 2002), its distribution represents the accessible volume for U6 and U4/U6 snRNPs in general. Twenty-five nuclei were reconstructed in three dimensions, following collection of 100 $0.1\text{-}\mu\text{m}$ optical z-sections per cell. Nuclear and nucleolar (negative SART3-GFP signal) volumes were calculated as described in the *Materials and Methods*. The volumes of all nucleoli from each cell were summed, and one nucleolar volume was recalculated to

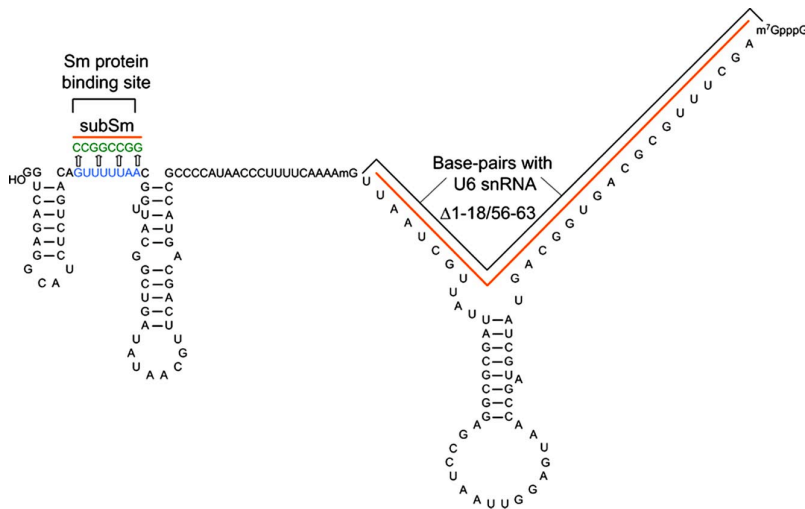


Figure 3. Secondary structure of U4 snRNA. The Sm protein and U6 binding sites are indicated by black brackets. In the U4SubSm mutant, the U-rich sequence of the Sm protein binding site was mutated by replacing it with a C- and G-rich region. In the U4 Δ 1-18/56-63 snRNA mutant, the U6 binding site was completely deleted, indicated by red lines. Modified from (Gerbi *et al.*, 2003).

simplify the simulation. The calculated average volume of the HeLa cell nucleus was $671.5 \pm 45.5 \mu\text{m}^3$ (mean \pm SEM), and the total nucleolar volume was $50 \mu\text{m}^3$ (7.5% of the nuclear volume). The nucleus and nucleolus were modeled as ellipsoids to provide generality (Figure 2B), and spherical CBs of varying numbers and sizes were added in the simulations that follow.

Next, it was necessary to determine the nuclear compartments available to U4 snRNA diffusion. Although we expect both snRNAs to diffuse throughout the HeLa cell nucleoplasm and concentrate in CBs, it has been reported that the U4 snRNA transits through nucleoli in *Xenopus* oocytes (Gerbi and Lange, 2002). We felt that the most sensitive approach to this question was microinjection of fluorescently labeled U4 snRNAs into the cytoplasm of HeLa cells and tracking their localization after assembly with Sm proteins and nuclear import. Runoff transcription of U4 snRNA constructs (Figure 3) was carried out with Alexa 488 rUTP in a ratio of 1:4, resulting in ~ 9 – 10 fluorescent molecules per transcript. Capped, fluorescently labeled RNAs were purified and injected into the cytoplasm of HeLa cells; and after 30–90 min of recovery, cells were fixed and stained for fibrillarlin (our unpublished data) and coilin to visualize nucleoli and CBs, respectively. Figure 4A shows that U4wt snRNA was imported into the nucleus and concentrated in CBs but that it was not detectable in nucleoli at any time point examined. As a negative control, a mutant lacking the Sm binding site (U4subSm; Figure 3) was injected and was not imported into the nucleus, as expected (Figure 4C) (Fischer *et al.*, 1994). A mutant U4 snRNA, which lacks U6 snRNA base-pairing sites (U4 Δ 1-18/56-63; Figure 3) and localizes to nucleoli in *Xenopus* oocytes (Gerbi *et al.*, 2003), accumulated in CBs but not in nucleoli (Figure 4B). Thus, U4 snRNA does not reside significantly in the nucleolus in human cells. In addition, these results confirm that U4 snRNA localizes to CBs independently of U6 snRNA binding, likely due to direct binding of Sm proteins to coilin (Gerbi *et al.*, 2003; Stanek and Neugebauer, 2004; Xu *et al.*, 2005).

Knowing the compartments available for U4 snRNP exploration, that U4 snRNP moves independently of U6 to CBs, and the HeLa cell nuclear volume, we are now able to ask how long it should take for a snRNP to reach a CB by diffusion. A Monte Carlo simulation was developed (see *Materials and Methods*) and applied to a random walk-and-

capture model. To validate the algorithm, the simulation was first used to compare the simulation results with the analytical solution solved for a simple sphere with a single target placed in its center (Kuthan, 2003). We considered a range of diffusion constants similar to those measured for RNPs of similar size and mobility to the U4 and U6 snRNPs: PAPB2 ($D = 0.6 \mu\text{m}^2/\text{s}$), U7 snRNP ($D = 1.0 \mu\text{m}^2/\text{s}$), and U1 snRNP ($D = 0.3 \mu\text{m}^2/\text{s}$) (Kues *et al.*, 2001; Calapez *et al.*, 2002; Handwerger *et al.*, 2003). Table 1 shows that two

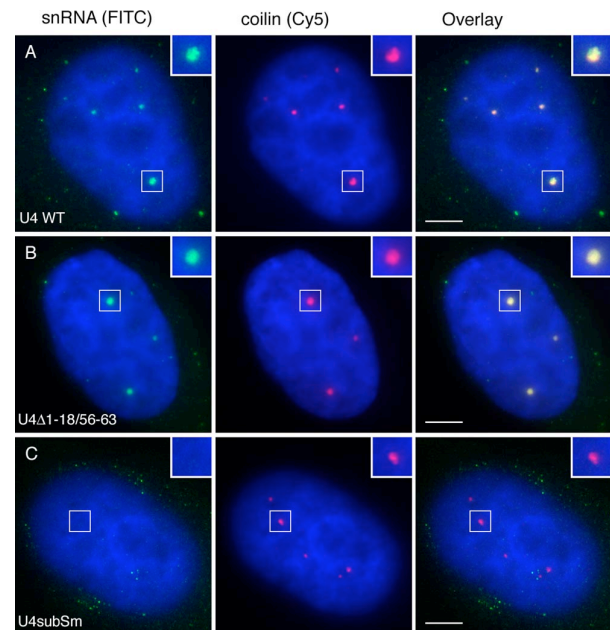


Figure 4. Microinjected U4 snRNA localizes specifically and independently to CBs. HeLa cells were microinjected into the cytoplasm with either U4wt snRNA (A); U4 Δ 1-18/56-63 snRNA, lacking sequences required for base-pairing with U6 snRNA (B), or U4subSm snRNA, lacking sequences required for Sm protein assembly (C). After 1-h recovery and fixation, cells were stained with anti-coilin antibody. The fluorescein isothiocyanate channel (green) shows Alexa 488-labeled snRNA, and the Cy5 channel (red) anti-coilin immunostaining. DAPI staining is shown in blue. Bar, $5 \mu\text{m}$.

Table 1. Mean FPT by random walk to the CB

D ($\mu\text{m}^2/\text{s}$)	$\langle\tau(r_0)\rangle$ (simulation in s)	$\langle\tau(r_0)\rangle$ analytical (solution in s)	Deviation from analytical solution (%)
0.2	364.0	344.2	+5.7
0.5	148.3	137.7	+7.7
1.0	75.7	69.9	+8.3

Random walk of a particle executed with three different D values within a sphere (radius of $5\ \mu\text{m}$) with a reflective boundary—the nucleus—and containing a perfectly absorbing target (radius of $0.5\ \mu\text{m}$) in the center—the CB. Mean first passage time ($\langle\tau(r_0)\rangle$) averaged over 1500 random starting positions and 400 runs per starting position is shown compared with the analytical solution with corresponding deviation.

methods yielded very similar results over a range of diffusion constants. The simulation was then applied to the “average” HeLa cell nucleus, described above. One to five CBs of radius $0.5\ \mu\text{m}$ were placed within the nuclear volume, touching neither the nuclear envelope nor the nucleolus. The nuclear envelope and nucleolar surface were modeled as reflecting surfaces, whereas CBs were totally absorbing. Figure 5 shows that the mean first passage time (FPT; $\langle\tau(r_0)\rangle$) for particle capture by a CB, depended on the number of CBs present. Interestingly, the presence of increasing numbers of CBs decreased the FPT; however, the asymptotic behavior of the FPT indicated that little benefit was achieved by the presence of more than three CBs. Because most tissue culture cells contain two to four CBs/nucleus, it would seem that this naturally occurring CB number is optimal.

We next sought to combine the results of the random walk simulation with the kinetics of U4 and U6 snRNP association in nucleoplasm and CBs, to determine whether snRNP targeting to CBs leads to more efficient snRNP assembly. To accomplish this aim, the snRNP concentration difference

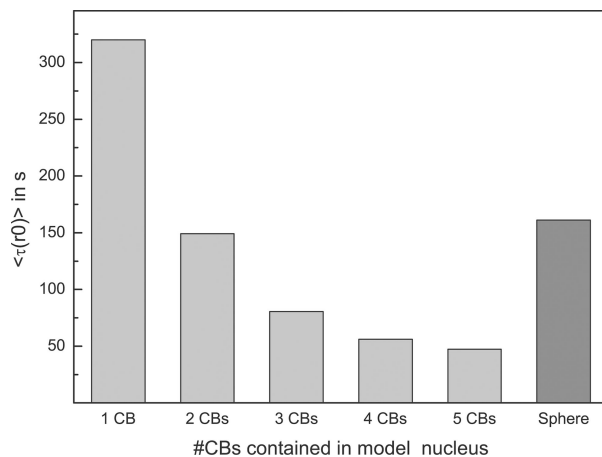


Figure 5. Influence of Cajal bodies on mean first passage time averaged over all initial positions [$\langle\tau(r_0)\rangle$]. The random walk simulation was executed in an average HeLa cell nucleus with different numbers of CBs. Light gray bars show [$\langle\tau(r_0)\rangle$] for a particle, with a diffusion coefficient of $0.5\ \mu\text{m}^2/\text{s}$, to find a CB in an average HeLa cell nucleus. Dark gray bar shows the analytical solution for a simplified spherical model possessing the same accessible volume with one CB in the center (Kuthan, 2003).

between CBs and nucleoplasm was a necessary parameter. Published values based on fluorescent in situ hybridization experiments vary from two- to fivefold, possibly reflecting difficulties with snRNA accessibility and/or incomplete probe hybridization (Carmo-Fonseca *et al.*, 1992; Matera and Ward, 1993; Schaffert *et al.*, 2004; Stanek and Neugebauer, 2004). Therefore, as a direct determination of snRNA concentration in CBs, we quantitated the fluorescent signals for the microinjected U4 snRNAs described above. The integrated fluorescent intensities of microinjected RNAs were measured in both compartments, and the relative average intensities were calculated. Three independent microinjections of U4wt and U4 Δ 1-18/56-63 snRNAs were carried out. Results shown in Figure 6A demonstrate that U4wt snRNA is 19.9 ± 1.3 -fold (mean \pm SEM) more concentrated in CBs than in the nucleoplasm. Interestingly, the U4 Δ 1-18/56-63 snRNA, which is unable to anneal with U6 snRNA, was concentrated 34.4 ± 2.1 -fold. These data suggest that the mutant U4 snRNA is trapped in the CB, because it cannot assemble into U4/U6 and U4/U6:U5 snRNPs, which would subsequently be released from CBs (Schaffert *et al.*, 2004; Stanek and Neugebauer, 2006).

To ensure that our determination of relative snRNA concentration in the CB versus the nucleoplasm was independent of the amount of U4 snRNA injected, we asked whether the obtained ratios for each CB depended on the total amount of snRNA injected into each cell. Therefore, integrated intensities over whole cells including cytoplasm were measured and compared with the obtained CB:nucleoplasm ratios (Figure 6B). By this measure, ~ 10 -fold variation in the delivered fluorescent snRNA was observed and is probably due to fluctuations in the duration of needle penetration of the plasma membrane. Linear least squares fitting of data points showed no correlation between CB:nucleoplasm ratio and injection amount, with p values of 0.831 and 0.830 for U4wt and U4 Δ 1-18/56-63 snRNAs, respectively, and where p is the probability that $R = 0$. The results clearly demonstrate that the ratio is independent of injection amount. Importantly, these observations indicate that U4 snRNP binding sites are not saturated over this 10-fold range, confirming the validity of the experimental approach. We conclude that endogenous U4 snRNA is concentrated in CBs 20-fold above nucleoplasm on average, with a range of 7- to 40-fold among individual CBs.

To determine whether the presence of CBs enhances U4/U6 snRNP assembly in the cell nucleus, the results of the simulation must be combined with a consideration of plausible association rates for the U4 and U6 snRNPs as they encounter one another in an aqueous environment. The association rate of two particles in solution depends on concentration, D , and the probability that the “hit” is productive. Because our simulation determines how long it will take for a single U4 snRNP to associate with any one of a number of U6 snRNPs, the concentration of U6 snRNPs was important. On average, a HeLa cell nucleus contains 4×10^5 copies of the U6 snRNA (Yu *et al.*, 1999). Of these, approximately one-third are present in U6 snRNPs (Bringmann *et al.*, 1984; Bell *et al.*, 2002). Therefore, we estimate the concentration of possible U6 snRNP targets in the nucleus to be 4×10^{-7} M. Although we have not directly measured the concentration differential between the CB and nucleoplasm for the U6 snRNP, we assume this is similar to the ratio determined above for the U4 snRNA; this is likely correct, because quantification of U4 and U6 snRNA in situ hybridization signals in HeLa cells produced similar results (Schaffert *et al.*, 2004). Finally, to factor in the probability that not every hit is productive, reactive patches defined by polar angles on

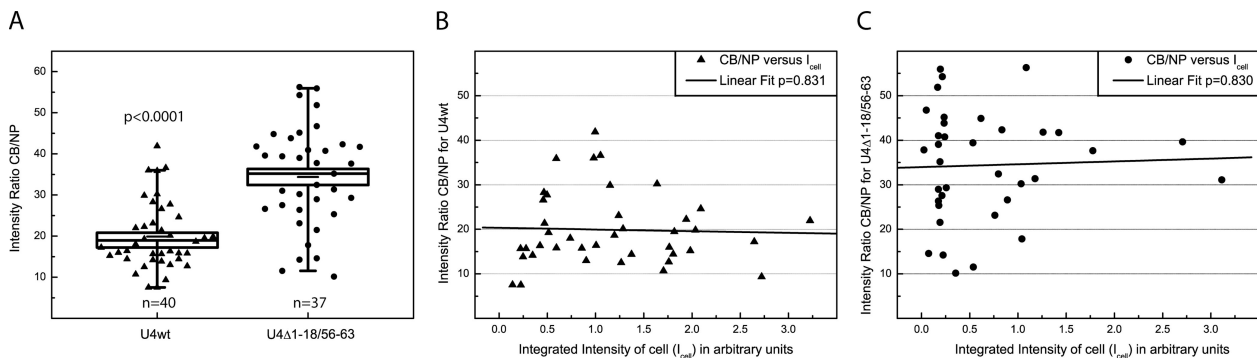


Figure 6. Concentration of U4 snRNA in the CB versus nucleoplasm. (A) Relative concentrations of U4 snRNA in CBs versus nucleoplasm. The cytoplasm of HeLa cells was microinjected with either U4wt ($n = 40$) or U4 Δ 1-18/56-63 ($n = 37$) snRNAs. After recovery and fixing, cells were stained with anti-coilin antibody. Fluorescent intensities in CBs, nucleoplasm, and background were measured and normalized. The ratios of each cell were averaged. The boxplot represents the pooled data of three independent experiments, each 11–15 cells. The graph depicts the 5–95 percentile distribution (whiskers) with the SE and mean represented by the box and horizontal line, respectively. The data points are scattered along the x -axis for visibility. A two-tailed Mann–Whitney test confirmed a highly significant difference ($p < 0.0001$) between the values for the two injected RNAs. (B and C) Intensity ratio CB/NP is not affected by the amount of injected fluorescent RNA. The sections of each injected cell were projected in one plane. The integrated intensity of the whole cell, including cytoplasm, was measured, and the signal of a similar area devoid of cells on the same slide was subtracted as background. Graphs show integrated intensities measured over individual cells (x -axis) versus corresponding CB/NP ratios (y -axis) for U4wt snRNA (B) and U4 Δ 1-18/56-63 snRNA (C). Linear least squares fitting showed that injected intensities are highly uncorrelated to the observed intensity ratio CB/NP ($p = 0.83$ and 0.831 , where p is the probability that $R = 0$).

the surface of each interacting sphere were calculated (see *Materials and Methods*). The results show that application of reactive patches to the prediction of productive hit frequency reduces the diffusion-limited association rate by ~ 4 orders of magnitude (Table 2), consistent with empirical studies of protein–ligand association in solution (Schreiber and Fersht, 1996).

By combining the results of the Monte Carlo simulation of a random walk and the calculated association rates, the effect of CBs on the rate of U4/U6 snRNP association could be determined for a variety of different conditions. Figure 7A shows the predicted rates for model cell nuclei containing one to four CBs, with an snRNA concentration difference of 20-fold between CB and nucleoplasm. In addition, the effect of CB size was assessed, because the radius of individual CBs can vary within single cells between 0.25 and 0.5 μm (Gall, 2000). The results show a U4 snRNP will need 1315 s to associate with a U6 snRNP in a cell lacking CBs. As increasing numbers of CBs are added to the nucleus, this time progressively declined to ~ 120 s for a nucleus containing four large CBs. It is currently not known what proportion of the 2×10^5 U4 snRNAs per cell are in U4 mono-snRNPs (Yu *et al.*, 1999); however, one can use the productive hit rate to project overall rates of U4/U6 snRNP assembly for possible values. For example, if 10% of total U4 were in mono-snRNPs, then the U4/U6 snRNP assembly

rate would be 15.2/s in a cell with no CBs, compared with 164 U4/U6 snRNPs/s in a cell with four large CBs. From the random walk simulation shown in Figure 5, it is clear that the progressive decline is due to the decrease in FPT to CB capture when more CBs are present. However, even a nucleus with a single large CB shows an enhanced association rate of 386 s. We conclude from this that, given the calculated association rates (see above), the presence of three to four CBs per nucleus yields a predicted 11-fold enhancement of productive hits between U4 and U6 snRNPs.

To address variation in the degree to which snRNAs are concentrated in CBs (see Figure 6), we also carried out the simulation in model nuclei containing three CBs (the average number of CBs per nucleus in the HeLa cell line we have used here) of different radius and containing different concentrations of snRNAs relative to nucleoplasm. Figure 7B shows that even if the concentration of the target (U6 snRNP) in CBs were only 5 times over nucleoplasm, assembly with U4 snRNP would be ~ 4 times faster than assembly in a nucleus without CBs. Note that the lowest snRNA concentration difference we measured for any CB in these cells was 7.5-fold. The association rates shown in both panels of Figure 7 were calculated for diffusion coefficients of 0.5 $\mu\text{m}^2/\text{s}$; however, because of the direct dependence of the simulation and the association rate on the diffusion coeffi-

Table 2. Calculation of association rates

D ($\mu\text{m}^2/\text{s}$)	k_D ($\text{M}^{-1} \text{s}^{-1}$)	k_{patch} ($\text{M}^{-1} \text{s}^{-1}$)	k_{NP} (s^{-1})	k_{CB} (s^{-1})
0.2	2.12×10^7	0.76×10^3	3.05×10^{-4}	6.10×10^{-3}
0.5	5.30×10^7	1.60×10^3	7.63×10^{-4}	15.26×10^{-3}
1.0	10.60×10^7	3.20×10^3	15.26×10^{-4}	30.51×10^{-3}

U4 snRNP–U6 snRNP association rates in the nucleoplasm and CB were calculated for three different D values. Collision rates (k_D), association rates (k_{patch}), and the association rates per cell per second in the nucleoplasm (k_{NP}) and CB (k_{CB}) are shown. The concentration of the target (U6 snRNP) was assumed to be 20-fold higher than the nucleoplasmic concentration.

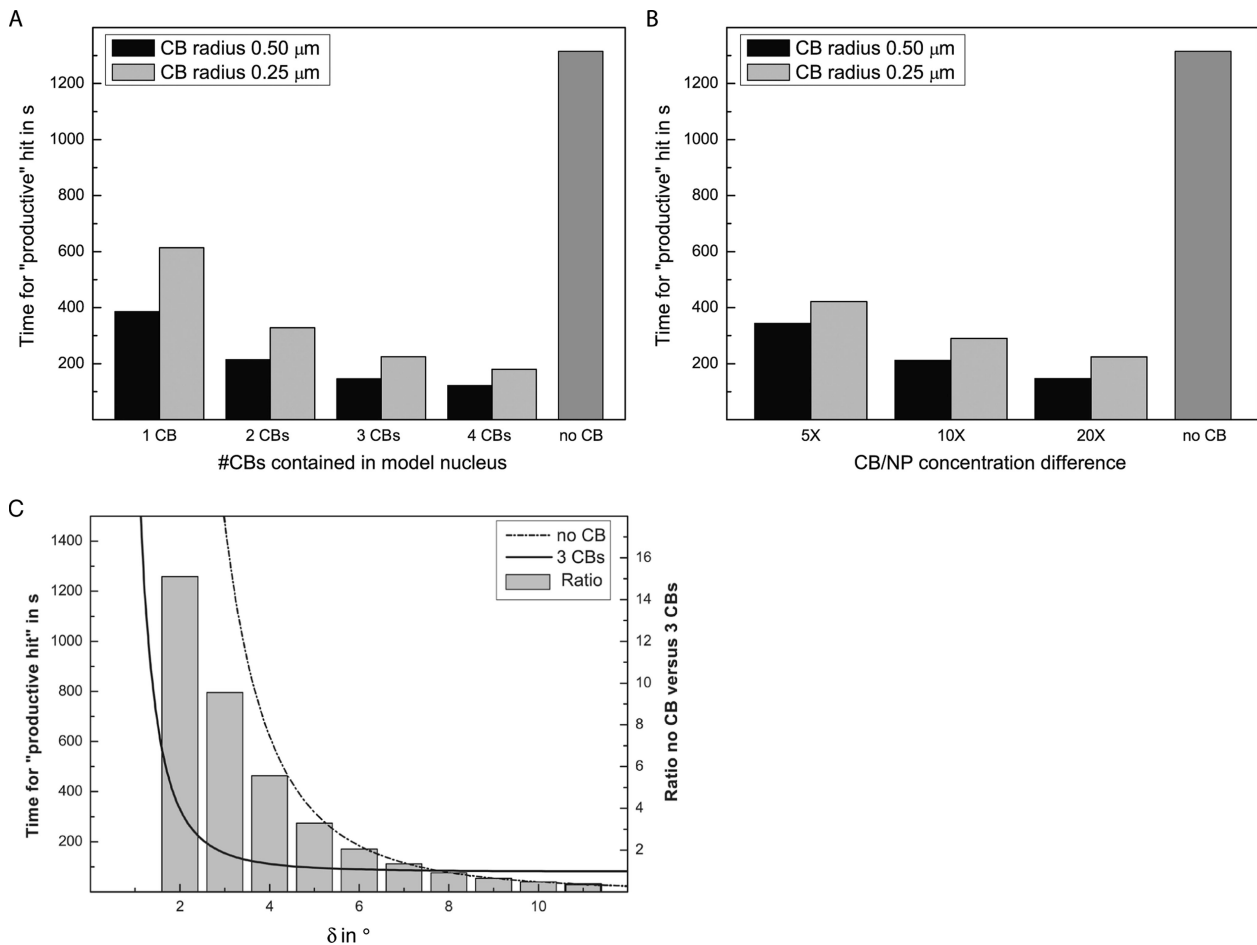


Figure 7. Cajal bodies enhance U4/U6 snRNP assembly over a plausible range in snRNA concentrations and CB numbers and sizes. Combining the simulation data with estimated association rates leads to a prediction of productive hits between U4 and U6 snRNPs, depicted here as time in seconds for one particle to have a productive hit. (A) Variation in association rates in model nuclei, containing one to four CBs in which snRNP targets are concentrated 20-fold over nucleoplasm. Independent solutions are shown for CBs of radius 0.5 (black bars) or 0.25 μm (light gray bars), compared with a cell without a CB (dark gray bar). (B) Variation in association rates in model nuclei, containing three CBs, in which snRNP targets are concentrated 5-, 10-, and 20-fold over nucleoplasm. Note that variation among the predicted values shown in the figure was <5%. (C) Dependence of productive hit rates on polar angle (δ) and resulting difference in overall di-snRNP assembly in a nucleus without CB compared with cell with three CBs. The solid line represents time for productive hits in seconds, in a nucleus with three CBs. The dashed line represents nucleus time for productive hits in seconds, in a nucleus without CBs. Gray bars represent the δ -fold difference in time to productive hit in a cell with three CBs compared with a cell with none. Parameters are $D = 0.5 \mu\text{m}^2/\text{s}$, three CBs (0.5- μm radius), and 20 times concentration difference CB/NP.

cient, the relative effect of CBs is the same for all diffusion coefficients. Therefore, this unbiased analysis shows that, owing to the concentration of U4 and U6 in the CB and given an average number of CBs per nucleus, the increased number of productive hits in CBs is predicted to enhance snRNP assembly rates by ~ 10 -fold.

Finally, we address the question of how the productive hit rate and therefore the enhancement of assembly by CBs would respond to changes in the reactive patch value. This reactive patch specifies the maximal rotational shift of the binding sites of two particles at close distance, at which a productive hit can occur (Vijayakumar *et al.*, 1998). As discussed above, the reactive patch value of 3° used for the simulations presented yielded association rates that match well with known association rates among protein binding partners as well as productive hit rates for RNA polymerase I interactions with its transcriptional target, rDNA

(Schreiber and Fersht, 1996; Dunder *et al.*, 2002). However, it is possible that the actual reactive patches on snRNPs are smaller or larger than those estimated here. Figure 7C shows that if the reactive patch value is only 2° , then the presence of CBs enhances snRNP assembly by ~ 14 -fold, with identical parameters to those used in Figure 7B. Larger reactive patch values result in a diminution of the enhancement by CBs, with the rates of association in cells with and without CBs becoming equal at $>7^\circ$. This large reactive patch value corresponds to an association rate 15 times faster than the rate used in our model; however, reactive patches of that size have not been reported and seem, together with the corresponding rapid rate of association, very unlikely. We conclude that, for reactive patch values yielding association rates that correspond with previous studies, the presence of CBs in nuclei are predicted to enhance the rate of U4/U6 snRNP assembly by ~ 1 order of magnitude.

DISCUSSION

Here, we have shown that mathematical modeling predicts an up to 11-fold enhanced rate of U4/U6 snRNP assembly when nuclei contain four CBs. The scenario addressed is one in which a U4 snRNP moves by random walk throughout the nucleoplasm until it either associates with a U6 snRNP in the nucleoplasm or is captured by a CB, where it experiences a higher concentration of U6 snRNPs with which it can associate. The model assumes 1) that U4 and U6 snRNPs are targeted independently to CBs (Gerbi *et al.*, 2003; Stanek *et al.*, 2003; Stanek and Neugebauer, 2004), which was further verified by microinjection experiments presented here and 2) that snRNPs move within the nucleus by diffusion, as reported previously (Kues *et al.*, 2001; Handwerger *et al.*, 2003). Additional elements were empirically derived, including a three-dimensional model of the living HeLa cell nucleus and a determination of the average snRNP concentration difference (~20-fold) in CBs versus nucleoplasm. This work provides a quantitative framework for modeling compartmentalized functions within the cell.

The modeling results relied on a random walk-and-capture simulation to determine how long it takes (FPT) for snRNPs diffusing throughout the nucleoplasm to encounter a CB. The expected shortening of the FPT with increasing CB numbers was asymptotic to a lowest value suggestive of an optimal CB number of three to four per nucleus. Remarkably, this predicted CB number coincides with the observed number of CBs per HeLa cell nucleus, suggesting CB numbers may be regulated among cells according to nuclear size and/or expression levels of CB components. Combination of these results with calculated association rates enabled the further prediction that CBs of varying sizes and numbers enhance the rate of U4-U6 snRNP association. For this, we used a range of diffusion constants, known numbers of snRNPs per cell, and a reactive patch model to estimate association rates. Given these parameters, we predict that individual U4 snRNPs would require ~20 min to assemble with a U6 snRNP in a nucleus lacking CBs, compared with only 2 min in a nucleus containing four large CBs. The time course of snRNP biogenesis *in vivo* is currently unknown; however, snRNPs are abundant and long lived (Yu *et al.*, 1999), such that an assembly process taking on the order of minutes is not out of the question.

snRNPs in living cell nuclei reside in CBs for some time (Dundr *et al.*, 2004), yet little is known about their dynamics within the CB. Very likely, the apparent diffusion constants of U4 and U6 snRNPs within CBs are also slower, owing to the binding of Sm proteins to coilin and the U6 snRNP component SART3 to its binding partner(s) in CBs (Handwerger *et al.*, 2003; Stanek *et al.*, 2003; Deryusheva and Gall, 2004; Xu *et al.*, 2005). The CBs of somatic cells are too small to permit determinations of diffusion constants for snRNPs with current methods; however, future technological developments may make this possible. Second, it is possible that snRNPs bound to coilin and/or other targets within the CB orient snRNPs, such that association between two snRNPs is favored. This scenario has been proposed for U4/U6 and U4/U6-U5 snRNP assembly and release from the CB, but thus far it has not been experimentally addressed (Stanek and Neugebauer, 2006). Thus, it is possible that snRNP association rates in CBs may be even higher than those estimated here, based purely on concentration differences.

These results on U4/U6 assembly in the CB provide new insight into the cellular advantage of concentrating molecules within a pathway into nonmembrane-bound compartments. Because the CB concentrates additional sets of mol-

ecules that participate in distinct assembly events, this work raises the possibility that rates of assembly of telomerase RNP, snoRNPs (small nucleolar RNP), and the histone 3' end processing machinery are all promoted in a similar manner by CBs (Stanek and Neugebauer, 2006). Indeed, dispersal of CB components by coilin depletion was recently shown to impair cell proliferation (Lemm *et al.*, 2006), suggesting that coilin expression facilitates a process (or processes) that is rate limiting for cell growth and division. Based on this work, we speculate that, like membrane-bound organelles, additional nonmembrane bound compartments observed throughout the cell—such as cytoplasmic P granules and P bodies, involved in translational regulation and RNA decay—may enhance the rates of association of key components of their respective machineries.

ACKNOWLEDGMENTS

We thank Karsten Kruse, Kahled Kairy, Jonathon Howard, Ivo Sbalzarini, Stephan Grill, Ernesto Di Iorio, Magdalena Strzelecka, and Arnold Kiss for helpful discussions and comments on the manuscript. We are grateful to Albrecht Bindereif for the wild-type human U4 snRNA clone and Maria Carmo-Fonseca for the gift of the anti-coilin mAb 5P10. This work was supported by Grant NE 909/1-1 from the Deutsche Forschungsgemeinschaft (to K.N.) and a Partner Group grant from the Max Planck Gesellschaft (to D.S.).

REFERENCES

- Almeida, F., Saffrich, R., Ansorge, W., and Carmo-Fonseca, M. (1998). Microinjection of anti-coilin antibodies affects the structure of coiled bodies. *J. Cell Biol.* **142**, 899–912.
- Andrade, L. E., Tan, E. M., and Chan, E. K. (1993). Immunocytochemical analysis of the coiled body in the cell cycle and during cell proliferation. *Proc. Natl. Acad. Sci. USA* **90**, 1947–1951.
- Bell, M., Schreiner, S., Damianov, A., Reddy, R., and Bindereif, A. (2002). p110, a novel human U6 snRNP protein and U4/U6 snRNP recycling factor. *EMBO J.* **21**, 2724–2735.
- Berg, H. (1993). *Random Walks in Biology*. Princeton, NJ: Princeton University Press.
- Berg, O. G. (1985). Orientation constraints in diffusion-limited macromolecular association. The role of surface diffusion as a rate-enhancing mechanism. *Biophys. J.* **47**, 1–14.
- Boudonck, K., Dolan, L., and Shaw, P. J. (1998). Coiled body numbers in the *Arabidopsis* root epidermis are regulated by cell type, developmental stage and cell cycle parameters. *J. Cell Sci.* **111**, 3687–3694.
- Boudonck, K., Dolan, L., and Shaw, P. J. (1999). The movement of coiled bodies visualized in living plant cells by the green fluorescent protein. *Mol. Biol. Cell* **10**, 2297–2307.
- Bringmann, P., Appel, B., Rinke, J., Reuter, R., Theissen, H., and Luhrmann, R. (1984). Evidence for the existence of snRNAs U4 and U6 in a single ribonucleoprotein complex and for their association by intermolecular base pairing. *EMBO J.* **3**, 1357–1363.
- Calapez, A., Pereira, H. M., Calado, A., Braga, J., Rino, J., Carvalho, C., Tavanez, J. P., Wahle, E., Rosa, A. C., and Carmo-Fonseca, M. (2002). The intranuclear mobility of messenger RNA binding proteins is ATP dependent and temperature sensitive. *J. Cell Biol.* **159**, 795–805.
- Carmo-Fonseca, M., Pepperkok, R., Carvalho, M. T., and Lamond, A. I. (1992). Transcription-dependent colocalization of the U1, U2, U4/U6, and U5 snRNPs in coiled bodies. *J. Cell Biol.* **117**, 1–14.
- Darzacq, X., Jady, B. E., Verheggen, C., Kiss, A. M., Bertrand, E., and Kiss, T. (2002). Cajal body-specific small nuclear RNAs: a novel class of 2'-O-methylation and pseudouridylation guide RNAs. *EMBO J.* **21**, 2746–2756.
- Deryusheva, S., and Gall, J. G. (2004). Dynamics of coilin in Cajal bodies of the *Xenopus* germinal vesicle. *Proc. Natl. Acad. Sci. USA* **101**, 4810–4814.
- Dundr, M., Hebert, M. D., Karpova, T. S., Stanek, D., Xu, H., Shpargel, K. B., Meier, U. T., Neugebauer, K. M., Matera, A. G., and Misteli, T. (2004). *In vivo* kinetics of Cajal body components. *J. Cell Biol.* **164**, 831–842.

- Dundr, M., Hoffmann-Rohrer, U., Hu, Q., Grummt, I., Rothblum, L. I., Phair, R. D., and Misteli, T. (2002). A kinetic framework for a mammalian RNA polymerase in vivo. *Science* 298, 1623–1626.
- Fischer, U., Heinrich, J., van Zee, K., Fanning, E., and Luhrmann, R. (1994). Nuclear transport of U1 snRNP in somatic cells: differences in signal requirement compared with *Xenopus laevis* oocytes. *J. Cell Biol.* 125, 971–980.
- Gall, J. G. (2000). Cajal bodies: the first 100 years. *Annu. Rev. Cell Dev. Biol.* 16, 273–300.
- Gerbi, S. A., Borovjagin, A. V., Odreman, F. E., and Lange, T. S. (2003). U4 snRNA nucleolar localization requires the NHPX/15.5-kD protein binding site but not Sm protein or U6 snRNA association. *J. Cell Biol.* 162, 821–832.
- Gerbi, S. A., and Lange, T. S. (2002). All small nuclear RNAs (snRNAs) of the [U4/U6.U5] Tri-snRNP localize to nucleoli: identification of the nucleolar localization element of U6 snRNA. *Mol. Biol. Cell* 13, 3123–3137.
- Handwerker, K. E., Murphy, C., and Gall, J. G. (2003). Steady-state dynamics of Cajal body components in the *Xenopus* germinal vesicle. *J. Cell Biol.* 160, 495–504.
- Howard, J. (2001). *Mechanics of Motor Proteins and the Cytoskeleton*, Sunderland, MA: Sinauer Associates.
- Jady, B. E., Darzacq, X., Tucker, K. E., Matera, A. G., Bertrand, E., and Kiss, T. (2003). Modification of Sm small nuclear RNAs occurs in the nucleoplasmic Cajal body following import from the cytoplasm. *EMBO J.* 22, 1878–1888.
- Kiss, A. M., Jady, B. E., Darzacq, X., Verheggen, C., Bertrand, E., and Kiss, T. (2002). A Cajal body-specific pseudouridylation guide RNA is composed of two box H/ACA snoRNA-like domains. *Nucleic Acids Res.* 30, 4643–4649.
- Kues, T., Dickmanns, A., Luhrmann, R., Peters, R., and Kubitscheck, U. (2001). High intranuclear mobility and dynamic clustering of the splicing factor U1 snRNP observed by single particle tracking. *Proc. Natl. Acad. Sci. USA* 98, 12021–12026.
- Kuthan, H. (2003). A mathematical model of single target site location by Brownian movement in subcellular compartments. *J. Theor. Biol.* 221, 79–87.
- Lemm, I., Girard, C., Kuhn, A. N., Watkins, N. J., Schneider, M., Bordonne, R., and Luhrmann, R. (2006). Ongoing U snRNP Biogenesis Is Required for the Integrity of Cajal Bodies. *Mol. Biol. Cell.*
- Matera, A. G., and Shpargel, K. B. (2006). Pumping RNA: nuclear bodybuilding along the RNP pipeline. *Curr. Opin. Cell Biol.* 18, 317–324.
- Matera, A. G., and Ward, D. C. (1993). Nucleoplasmic organization of small nuclear ribonucleoproteins in cultured human cells. *J. Cell Biol.* 121, 715–727.
- Misteli, T., Caceres, J. F., and Spector, D. L. (1997). The dynamics of a pre-mRNA splicing factor in living cells. *Nature* 387, 523–527.
- Nesic, D., Tanackovic, G., and Kramer, A. (2004). A role for Cajal bodies in the final steps of U2 snRNP biogenesis. *J. Cell Sci.* 117, 4423–4433.
- Northrup, S. H., and Erickson, H. P. (1992). Kinetics of protein-protein association explained by Brownian dynamics computer simulation. *Proc. Natl. Acad. Sci. USA* 89, 3338–3342.
- Platani, M., Goldberg, I., Swedlow, J. R., and Lamond, A. I. (2000). In vivo analysis of Cajal body movement, separation, and joining in live human cells. *J. Cell Biol.* 151, 1561–1574.
- Politz, J. C., Tuft, R. A., Prasanth, K. V., Baudendistel, N., Fogarty, K. E., Lifshitz, L. M., Langowski, J., Spector, D. L., and Pederson, T. (2006). Rapid, diffusional shuttling of poly(A) RNA between nuclear speckles and the nucleoplasm. *Mol. Biol. Cell* 17, 1239–1249.
- Schaffert, N., Hossbach, M., Heintzmann, R., Achsel, T., and Luhrmann, R. (2004). RNAi knockdown of hPrp31 leads to an accumulation of U4/U6 di-snRNPs in Cajal bodies. *EMBO J.* 23, 3000–3009.
- Schreiber, G., and Fersht, A. R. (1996). Rapid, electrostatically assisted association of proteins. *Nat. Struct. Biol.* 3, 427–431.
- Shav-Tal, Y., Darzacq, X., Shenoy, S. M., Fusco, D., Janicki, S. M., Spector, D. L., and Singer, R. H. (2004). Dynamics of single mRNPs in nuclei of living cells. *Science* 304, 1797–1800.
- Shpargel, K. B., and Matera, A. G. (2005). Gemin proteins are required for efficient assembly of Sm-class ribonucleoproteins. *Proc. Natl. Acad. Sci. USA* 102, 17372–17377.
- Stanek, D., and Neugebauer, K. M. (2004). Detection of snRNP assembly intermediates in Cajal bodies by fluorescence resonance energy transfer. *J. Cell Biol.* 166, 1015–1025.
- Stanek, D., and Neugebauer, K. M. (2006). The Cajal body: a meeting place for spliceosomal snRNPs in the nuclear maze. *Chromosoma* 115, 343–354.
- Stanek, D., Rader, S. D., Klingauf, M., and Neugebauer, K. M. (2003). Targeting of U4/U6 small nuclear RNP assembly factor SART3/p110 to Cajal bodies. *J. Cell Biol.* 160, 505–516.
- Stark, H., Dube, P., Luhrmann, R., and Kastner, B. (2001). Arrangement of RNA and proteins in the spliceosomal U1 small nuclear ribonucleoprotein particle. *Nature* 409, 539–542.
- Vijayakumar, M., Wong, K. Y., Schreiber, G., Fersht, A. R., Szabo, A., and Zhou, H. X. (1998). Electrostatic enhancement of diffusion-controlled protein-protein association: comparison of theory and experiment on barnase and barstar. *J. Mol. Biol.* 278, 1015–1024.
- Wersig, C., and Bindereif, A. (1990). Conserved domains of human U4 snRNA required for snRNP and spliceosome assembly. *Nucleic Acids Res.* 18, 6223–6229.
- Xu, H., Pillai, R. S., Azzouz, T. N., Shpargel, K. B., Kambach, C., Hebert, M. D., Schumperli, D., and Matera, A. G. (2005). The C-terminal domain of coilin interacts with Sm proteins and U snRNPs. *Chromosoma* 114, 155–166.
- Yu, Y.-T., Sharl, E. C., Smith, C. M., and Steitz, J. A. (1999). The growing world of small nuclear ribonucleoproteins. In: *The RNA World*, ed. C. Gesteland, and Atkins, Cold Spring Harbor, NY: Cold Spring harbor Laboratory Press, 487–524.
- Zhou, H. X. (1993). Brownian dynamics study of the influences of electrostatic interaction and diffusion on protein-protein association kinetics. *Biophys. J.* 64, 1711–1726.